Optics and Lasers in Engineering 49 (2011) 1254–1263

Contents lists available at ScienceDirect

Optics and Lasers in Engineering

journal homepage: www.elsevier.com/locate/optlaseng

Digital particle holographic system for measurements of spray field characteristics

Yan Yang [a], Bo-seon Kang [b,*]

[a] Key Laboratory of Automobile Parts and Test Techniques (Chongqing University of Technology), Ministry of Education, Chongqing, China
[b] Department of Mechanical Engineering, Chonnam National University, 333 Yongbong-ro, Buk-gu, Gwangju 500-757, Korea

ARTICLE INFO

Article history:
Received 22 January 2011
Received in revised form
27 May 2011
Accepted 23 June 2011
Available online 18 July 2011

Keywords:
Digital particle holography
Characteristics of spray droplets
Image processing
Uncertainty analysis

ABSTRACT

A digital particle holographic system for measurements of spray fields is presented. A double exposure hologram recording system with a synchronization system for time control is established, resulting in digital holograms that can be quickly recorded. To process recorded holograms, the correlation coefficient method is used for focal plane determination of particles. To remove noise and improve the quality of holograms and reconstructed images, a Wiener filter is adopted. The two-threshold and image segmentation methods are used for binary image transformation. For particle pairing, the match probability method is adopted. The proposed system is applied to a spray field, and three-dimensional velocities and sizes of spray droplets are measured. Measurement results from the digital holographic system are compared to those made by laser instruments, which prove the feasibility of the proposed in-line digital particle holographic system as a good measurement tool for spray droplets.

© 2011 Elsevier Ltd. All rights reserved.

1. Introduction

The particle flow fields encountered in many areas of engineering have numerous complexities and irregularities, and a three-dimensional (3-D) nature. To investigate the characteristics of such fields, various measurement techniques and instruments have been developed and commercialized. Among these, non-intrusive optical instruments such as the laser Doppler velocimeter (LDV), the phase Doppler particle analyzer (PDPA), and the particle image velocimeter (PIV) have advanced remarkably due to advances in lasers, imaging systems, and computers.

The LDV and PDPA are commonly used as laser instruments for particle flow fields and offer reliable 3-D information based on vast amounts of sampling, but are limited as point measurement methods [1]. PIV and particle tracking velocimetry (PTV), which can detect particles in a two-dimensional (2-D) plane with a simple optical configuration, can overcome this problem [2], but they cannot measure the velocity component normal to the plane as an imaging technique. Therefore, a measurement tool capable of determining 3-D features of particles over a complete test volume as a function of time remains to be developed.

As for spray diagnostic systems, considerable progress has been made in laser instrument technologies, making it possible to obtain reliable data on droplet sizes and velocities in dilute spray regions. However, most of these methods are inherently limited in dense spray regions where liquid elements are rather large and non-spherical. In addition, no information on spray structure can be provided by these kinds of instruments.

Holography is a technique that allows the light scattered from an object to be recorded and later reconstructed, thereby appearing as if the object is in the same position relative to the recording medium as when the recording was made. It can instantaneously capture volumetric information from 3-D fields. The holographic technique reproduces the frozen spray as a 3-D image, from which droplet sizes and positions, 3-D velocities, and spray structures can be easily investigated [3,4].

Due to the rapid development of charge-coupled devices (CCDs) and computers, digital holography (DH) has rapidly taken the place of conventional optical holography. Its advantages are as follows: it does not need a wet process for developing recording media; the image recording procedure is easy for 3-D images of objects, and focused images of 3-D object at exact focal planes can be easily obtained by a computer without a mechanical focusing process. Based on advantages including high efficiency, simplicity, and real time analysis, digital holography has been widely used in spray measurement.

Muller et al. showed the potential of digital holography applied to measurements of spray droplets [5]. Palero et al. compared digital holography with digital image plane holography (DIPH), and they proved the capability of DH [6]. The results obtained by their experiments and processing methods showed that digital

* Corresponding author. Tel.: +82 62 530 1683; fax: +82 62 530 1689.
E-mail addresses: yangyan@cqut.edu.cn (Y. Yang), bskang@chonnam.ac.kr (B.-s. Kang).

0143-8166/$ - see front matter © 2011 Elsevier Ltd. All rights reserved.
doi:10.1016/j.optlaseng.2011.06.017

holography is well suited for droplet characterization only with the low droplet concentration and the sizing accuracy of DH was not as good as with DIPH. For the dense droplets, Lee et al. and Miller et al. added a separate reference beam to solve the problem of beam obscuration in dense sprays [7–9].

In this study, a simple in-line digital particle holographic system to measure spray fields is developed. Some special methods to enhance the measurement capability of digital holographic system are developed. To remove noises and improve the quality of holograms and reconstructed images, the Wiener filter was introduced. The correlation coefficient method was used to accurately determine the focal plane of droplets. The two-threshold and image segmentation methods were used to obtain high quality binary images from which we can get good results of droplet sizing and velocity measurements. Based on the developed system and processing methods, 3-D velocities and diameters of spray droplets under different spray conditions were measured. Finally, the measurement results obtained using the digital particle holographic system were compared with results from conventional instruments such as PDPA.

2. General principles

Digital holography is classified as in-line or off-axis depending on the optical setup. Compared with off-axis holography, in-line digital holography has high phase sensitivity, the simpler experimental setup, a less stringent requirement for spatial coherence and applicability to a wider class of sample geometries [10]. These benefits make the in-line holography very appealing, though in-line holography has lower resolution, which may limit its application in some cases.

The concept of in-line digital holography is shown in Fig. 1. An expanded laser beam goes through the object field. The part of the beam diffracted by objects and arriving at the recording surface is called the object beam, and the beam arriving without distortion from objects is called the reference beam. The superposition of two beams creates an interference pattern on a CCD sensor; this diffraction can be described by the Fresnel–Kirchhoff integral [11]

$$R(\xi',\eta') = \frac{i}{\lambda}\int_{-\infty}^{\infty}\int_{-\infty}^{\infty} h(x,y)E_R(x,y)\frac{\exp(-i(2\pi/\lambda)\rho)}{\rho}\,dx\,dy \quad (1)$$

with

$$\rho = \sqrt{(\xi'-x)^2+(\eta'-y)^2+d^2} \quad (2)$$

where $R(\xi',\eta')$, $h(x,y)$, $O(\xi,\eta)$ and $E_R(x,y)$ are functions of the reconstruction image, hologram, object, and reference, respectively. Here, d is the distance between two adjacent planes, λ is the wavelength, and ρ is the distance between two corresponding points in two adjacent planes. The coordinates appearing in Eqs. (1) and (2) are shown in Fig. 2.

The resolution of reconstruction images is related to the value of numerical aperture (NA), which consists of the CCD size and the object distance [12]. When the hologram is recorded on a large screen, optimal resolution can be achieved both laterally and in depth. Also the object, which is closer to the CCD the resolution of image is clearer [13]. The reconstruction image $R(\xi',\eta')$ can be obtained by the Fresnel method or the convolution

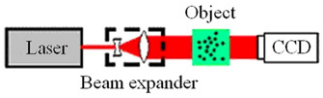

Fig. 1. Principle of in-line digital holography.

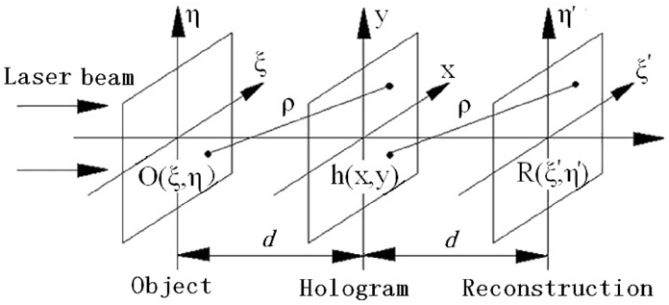

Fig. 2. Coordinate system.

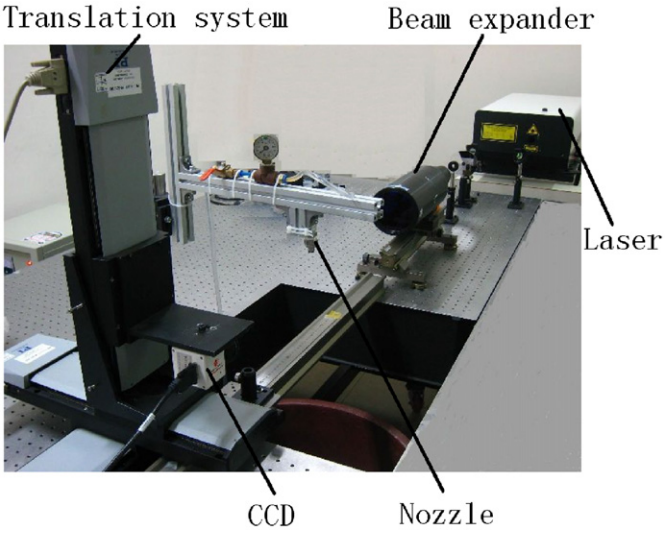

Fig. 3. Digital particle holographic system.

method [11]. In our previous analysis [13], the resolution of the reconstruction image by the convolution method was better than that by the Fresnel method. Therefore, the convolution method was used in this study. The mathematical expression of the convolution method is

$$R(\xi',\eta') = F^{-1}\left\{F[h(x,y)]\cdot F\left[\frac{i}{\lambda}\frac{\exp[-i(2\pi/\lambda)\sqrt{(d^2+(x-\xi')^2+(y-\eta')^2}]}{\sqrt{(d^2+(x-\xi')^2+(y-\eta')^2}}\right]\right\} \quad (3)$$

where $F[\ ]$ and $F^{-1}[\ ]$ are a Fourier transform and an inverse Fourier transform, respectively.

3. Digital particle holographic system

3.1. Hologram recording system

A digital particle hologram recording system for capturing spray holograms was established as shown in Fig. 3. The laser through the beam expander extends to a plane beam that generates spray holograms on a CCD, which has no lens. After collecting the holograms from the CCD, the hologram image can be reconstructed, and information of spray field can be extracted. The specifications of the system components are as follows:

Laser: Nd-YAG laser (Quantel, wavelength 532 nm).
CCD camera: Megaplus II ES4020 (Kodak, pixel size 7.4 μm, pixel number 2048 × 2048).

Pulse generator: 555 (Berkeley, 4 channels).
Translation system: M-531 (Physik Instrumente, precision: 33 nm).
Nozzle: Commercial nozzle (Spraying systems).

The control diagram of the synchronization system for the laser and the CCD camera is shown in Fig. 4. The flashlamps of laser were driven by two asynchronous pulse trains from the pulse generator. Each laser fires at Q-switches, with the laser 2 delayed with respect to the laser 1. When the laser fires, the pulse generator sends a single shot signal to the CCD camera, and then the CCD camera starts double exposure procedure. If two lasers fire in the first and second exposure intervals of the CCD camera, two images can be obtained. As indicated in Fig. 4, the time interval of double exposure holograms, Δt, is equal to $\Delta t_3 - \Delta t_1$.

3.2. Extraction of droplet features

3.2.1. Noise removal

The extraction of droplet features occurs in three steps. The first step is pre-processing, which enhances the quality of the holograms. Actual digital holograms contain many inherent noise sources due to various optical conditions and dust on components. Therefore, an image processing technique to eliminate this noise must be applied. To remove noise in holographic images, various filtering methods were examined including the inverse filter [14], the subtraction method [15], the Gaussian high pass filter [16], the spectral filter [17], and average filter [18], which is considered as the best one in digital holography.

In this study, the self-adaptive Wiener filter [19], which can effectively eliminate noise, was used in digital holography for the first time. The Wiener filter performs 2-D adaptive noise removal filtering. In digital holograms, the Wiener filter uses a pixel-wise adaptive method based on statistics estimated from a local neighborhood of each pixel. Here, the effect of the Wiener filter for noise removal was verified by checking whether it is beneficial to determination of the focal plane using the correlation coefficient method (this method will be discussed in the next section).

We used the hologram of the dot array target to verify the feasibility of the Wiener filter. Based on our CCD size, the hologram including 81 dots can be recorded. After application of the Wiener filter, the focal planes of each dot were obtained by the CC method. The mean value of the focal planes is assumed as the best focal plane of the target, which can be regarded as the real position of the target from the CCD camera. The error is defined as the difference between the predicted focal plane of each dot and the mean value of the focal planes.

Fig. 5(a)–(c) shows that the errors of focal plane determination by application of the Wiener filter to different steps of hologram processing. The results show that the Wiener filter was better when it was used twice for the pre-processing of holograms and the post-processing of reconstruction images. That is different from the conventional use of the filter in digital holography, namely, the application of the filter only to the pre-processing of holograms. To further verify the feasibility of the Wiener filter, we applied the average filter and the CC method to the same hologram and the errors are shown in Fig. 5(d). The comparison

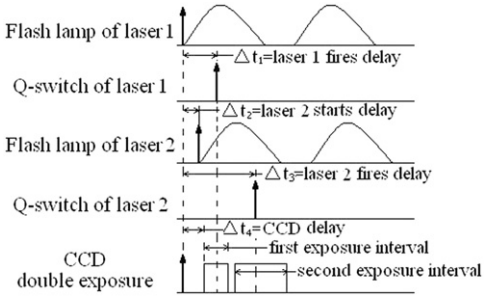

Fig. 4. Control diagram of synchronization system.

Table 1
Effect of the Wiener filter on the errors of focal plane determination.

	Object distance, d (mm)	Mean of focal planes (mm)	Mean of errors (μm)	Standard deviation of errors (μm)
Without filtering	155.799	155.824	10.790	7.375
With filtering		155.799	4.235	4.080

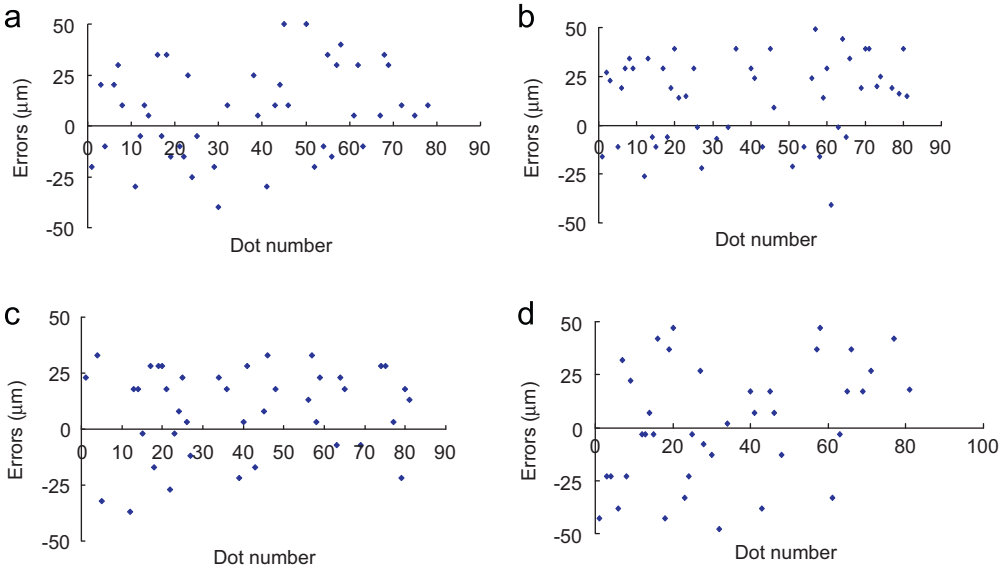

Fig. 5. Errors of focal plane determination using the Wiener filter (a, b, and c) and the average filter (d); (a) for hologram only, mean error=19.7 μm, (b) for reconstruction image only, mean error=21.98 μm, (c) for hologram and reconstruction image, mean error=18.69 μm, and (d) for hologram and reconstruction image, mean error=25.05 μm.

of the Wiener filter and the average filter indicates that the effect of the Wiener filter is better than that of the average filter. The effectiveness of the Wiener filter is also shown in Table 1. The Wiener filter can greatly reduce the error of the focal plane determination, which proves that the filter has an excellent ability to reduce noises in holograms or reconstruction images.

3.2.2. Determination of focal plane

The second step is the determination of the 3-D positions of spray droplets in reconstruction images. The x and y coordinates are easy to locate with high precision by the common image processing methods regardless of whether the droplets are in focus or unfocused. The main problem is how to find the location of the best focal plane of droplets along the optical axis; i.e., the z coordinate of the particle. Various methods have been suggested to determine the focal plane. Lefebvre et al. showed that the maximum modulus of the wavelet transform were reached at the best focal plane [20]. Dubois et al. introduced a method that uses the score of the integrated amplitude modulus [21]. Presently, the gradient method was regarded as a conventional solution and widely used in many researches [22]. In this study, the correlation coefficient method, which was first presented by Choo et al. in our research group, was used to determine the focal plane of particles [23,24].

The correlation coefficient between images measures the degree to which the two images are similar. The value of the correlation coefficient approaches 0 if there is no similarity between images, and approaches 1 if there is perfect similarity. The correlation coefficient is defined as

$$CC = \left[\frac{\sum_{m=1}^{M}\sum_{n=1}^{N}(F_{mn}-\overline{F})(G_{mn}-\overline{G})}{\sqrt{[\sum_{m=1}^{M}\sum_{n=1}^{N}(F_{mn}-\overline{F})^2][\sum_{m=1}^{M}\sum_{n=1}^{N}(G_{mn}-\overline{G})^2]}} \right] \quad (4)$$

where F and G are two images, m and n are the pixel indices, F_{mn} and G_{mn} are the gray levels of individual pixels of image F and G, respectively, and $\overline{F}$ and $\overline{G}$ are the mean gray levels of F and G, respectively. The image can be denoted by a matrix in the program, so the values of F_{mn} and G_{mn} and F and G, can easily be obtained after we import the image into the program. Fig. 6 shows a schematic of how to determine the focal plane of particles using correlation coefficients. A series of images are reconstructed slice-by-slice with a reconstruction interval Δz. The correlation coefficient at an arbitrary plane along the optical axis was evaluated using two images at the same distance as half of the correlation interval, $\Delta C_z/2$, from that plane. The focal plane (i.e., the z coordinates of the object) can be determined by choosing the peak point from the correlation coefficient curve.

Using the simulation particle hologram, which has the exact object distance, we compared the correlation coefficient method with the conventional gradient method to determine the focal plane of particles with different sizes and object distances. The error is defined as the difference between the predicted focal plane and the real object distance. The errors by the two methods at different particle sizes and object distances are shown in Table 2. All errors by the gradient method are much bigger than those of the CC method except a few points. The average of the errors for each particle size obtained by the two methods is compared in Fig. 7. The results show clearly that the CC method is superior to the classical gradient technique and it has higher accuracy.

In this study, considering the measurement accuracy and efficiency of calculation, the reconstruction interval, Δz, was chosen as 10 μm. At this reconstruction interval, the error, which is defined as the difference between the object distance and the predicted focal plane, can be expressed as $e = \pm n \times \Delta z/2 = \pm n5\,\mu m$, $n = 0, 1, 2, \ldots$. The half of Δz is introduced because the focal plane is located in the middle of two image planes when the CC curve has

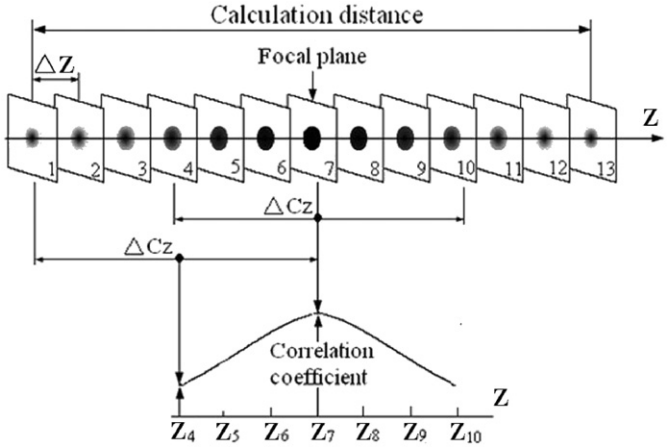

Fig. 6. Schematic diagram of the correlation coefficient method.

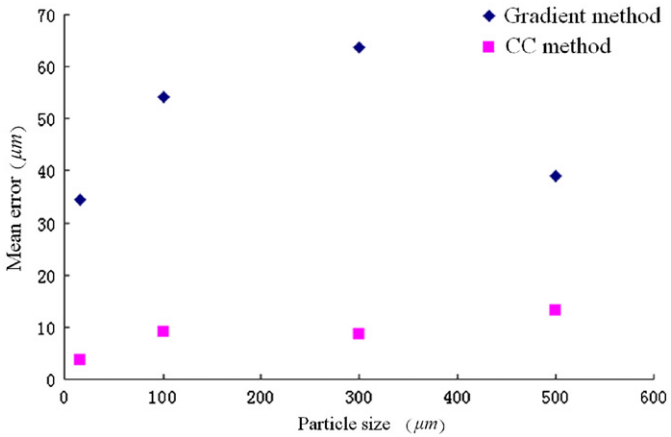

Fig. 7. Comparison of errors for the CC and gradient methods.

Table 2
Errors of focal plane determination by the correlation coefficient (CC) method and gradient (G) method (unit: μm).

Size, D_d (μm)	Object distance, d (mm)													
	150		170		200		220		240		300		400	
	CC	G	CC	G	CC	G	CC	G	CC	G	CC	G	CC	G
16	10	40	0	90	0	50	0	10	0	90	−20	10	10	−10
100	0	40	0	−70	0	−30	5	70	10	−70	−20	25	30	90
300	0	10	0	20	0	90	0	−90	15	90	−30	50	30	90
500	−10	20	10	20	5	10	10	10	20	30	−30	80	25	80

two consecutive peaks. From the viewpoint of application to particle measurements, the level of error less than 20 μm is fully acceptable for our purpose. If higher accuracy is required, the reconstruction interval can be reduced with the sacrifice of much longer calculation time.

3.2.3. Binarization of droplet images

The third step is the binarization of the reconstruction images. The reconstruction image of a hologram is the gray image, and it is difficult to extract the sizes of droplets. Therefore, an image conversion process that converts gray images to binary images must be achieved. To obtain clear particle images, appropriate threshold values should be determined to transform gray images to binary images. In this study, the two-threshold method was applied to obtain the optimal threshold [13]. The first threshold value, I_{th1}, was obtained as follows:

$$I_{th1} = I_{1\min} + \bar{I}_1 \tag{5}$$

Where $I_{1\min}$ and $\bar{I}_1$ are the minimum and average gray values of the reconstruction image, respectively. For the second threshold value, I_{th2}, the pixels whose gray values were under I_{th1} were selected first, comparing I_{th1} with the gray values of every pixel. The new minimum and average gray values of these pixels are $I_{2\min}$ and $\bar{I}_2$, respectively. The second threshold value is obtained as

$$I_{th2} = I_{2\min} + \bar{I}_2 \tag{6}$$

Using the second threshold value, we can transform gray images to binary images. In our validation experiments, a reconstruction image of a calibration target hologram was converted into the binary image using this method. The comparison results between the measured size and the actual size showed that the maximal and minimal errors were 7.3% and 0.2%, respectively, which proves the feasibility of the two-threshold method.

Some useful information about particles can be lost if only one threshold is applied to the entire image because the intensity of the reconstruction image is not uniform. Thus, an image segmentation method was used in this study. The entire image was divided into several small regions that were converted to binary images using respective thresholds obtained by the two-threshold method. The comparison experiments clearly demonstrate that the image obtained by locally different thresholds was better than that by one threshold. The next problem is how to determine the optimal number of segmentations in one image. Comparison of results for different segmentations showed that the number is smaller and the quality of the conversion image is poor. However, the increase of segmentations requires more calculation time. Considering all these factors, the optimum number of segmentations was chosen as 16.

3.2.4. Particle tracking algorithm

After the 3-D coordinates of every particle in each of two images were obtained, the fourth step, pairing process, was executed. Many efficient methods have been developed for particle pairing. In this study, the match probability method [25] for 2-D was used because of advantages such as reliability, efficiency, and ease of programming. The pairing algorithm is based on neighboring match probability and has more potential in particle matching. The method is mainly grounded in maximum velocity theory and quasi-rigidity conditions. Based on the principles of this method, the program of particle pairing in 3-D space was easily extended after adding one more dimension.

To verify the feasibility of the 3-D pairing program, a numerical simulation was conducted. First, a 3-D coordinate data file of 100 arbitrary particles was established. Then, these coordinates were changed as in real spray case. After two 3-D coordinate data files were obtained, the 3-D pairing program was applied and the pairing results were obtained. The pairing errors are defined as the difference between the measured distance of pairing particles and the actual moving distance. The error of 74% of the particles was zero. Therefore, the 3-D pairing program appeared to have worked properly.

3.2.5. Sizing

The last step is sizing. Using the z coordinates of droplets, the holograms were reconstructed and the focused images of corresponding droplets were obtained. After binarization of the images, the program automatically outlined the droplet and measured its size. The edge of a droplet was located, and the number of pixels inside the edge was counted. The properties of droplet size such as area and equivalent diameter were then calculated.

3.3. Procedure of hologram image processing

Based on the above methods, Fig. 8 shows a flow chart of hologram image processing. The procedure is as follows:

(1) Select the measurement object and set all necessary parameters such as wavelength, pixel size, reconstruction distance, and the pixel number, and then input the double holograms.
(2) Use the Wiener filter, thereby eliminating noise in the holograms.
(3) Reconstruct double exposure holograms using the convolution method.
(4) Use the Wiener filter to eliminate noise in the reconstruction images.
(5) Obtain binary images by appropriate threshold and image segmentation methods.
(6) Determine the x and y coordinates of particles regardless of whether or not the image is in focus. For every region including one particle, the correlation coefficient method is

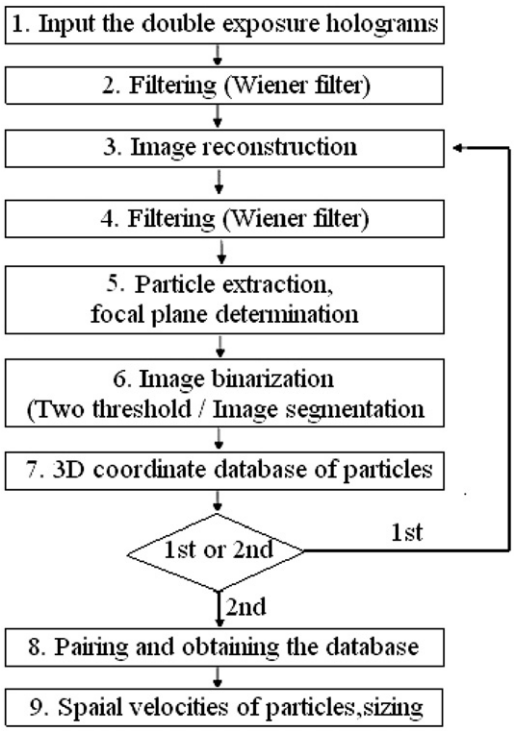

Fig. 8. Flow chart of hologram processing.

applied to calculate the focal plane, and the z coordinate and the size of the particle are obtained.
(7) Make a 3-D coordinate database of particles in double exposure images.
(8) Use the pairing method to obtain a database of pairing particles.
(9) Obtain 3-D velocities of spray droplets.

4. Experiments for spray field

4.1. Spray experiments

Using the digital particle holographic system described in Section 3, measurement experiments for a spray field at different conditions were conducted. The common spray nozzle is directly connected to the pressurized tank, which is full of the water and pressurized air. The injection pressures of spray were 14.7, 19.6, and 29.4 kPa. The time interval of double exposure holograms, Δt, is 150 μs and the laser pulse duration, i.e., the exposure time is 7 ns.

To obtain the distribution of actual velocities of the spray field, holograms of six regions were captured by a CCD camera. The six positions are shown in Fig. 9. At every region and pressure, ten holograms (five double exposures) were captured. A total of 180 holograms were obtained, which is enough to analyze the spray field. Typical double exposure holograms of droplets and reconstruction images are shown in Fig. 10.

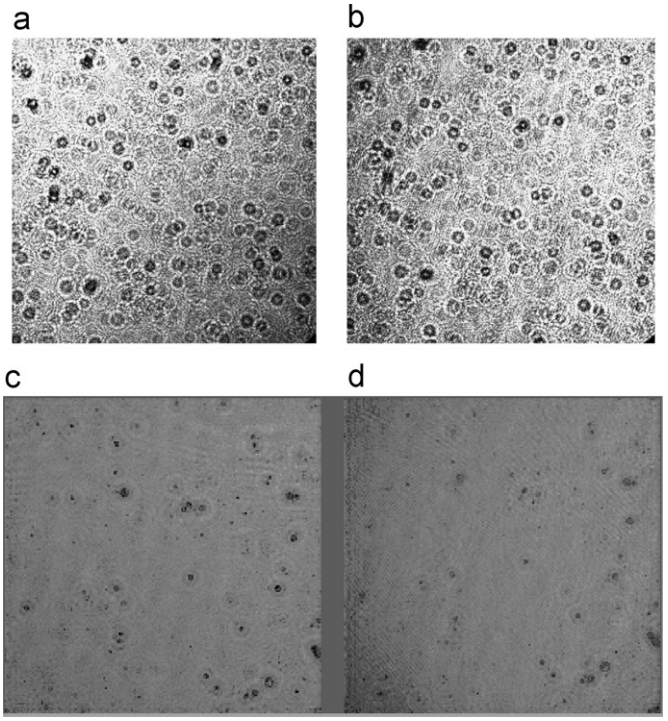

Fig. 10. Typical spray holograms and reconstruction images (position 1 at $P=14.7$ kPa); (a) and (b) first and second exposure holograms, and (c) and (d) reconstruction images corresponding to (a) and (b).

4.2. Extraction of droplet velocities

Using the image processing procedure presented in the previous section, the 3-D coordinates and the velocities of droplets are easily obtained. The distribution of droplet velocities in Fig. 10 is shown in Fig. 11. Combining all holograms and using the programs presented in Section 3, the 3-D coordinates and the velocities of droplets in different regions of the spray field were obtained. In practice, the main representation of droplet velocity is the absolute velocity, which indicates the speed of the droplet velocity. The absolute velocities of droplets at different regions and pressures are shown in Fig. 12. The behavior of droplets shown in Fig. 12 is consistent with the actual situation expected in a spray field. The droplet velocity was directly proportional to the applied injection pressure, and inversely proportional to the distance from the nozzle to the position of the droplet. If the regions are symmetric with respect to the center axis of the spray field, their absolute velocities are similar. At the same distance from the nozzle, the absolute velocities in the horizontal direction (V_x and V_z) at the spray axis are slow, and they become fast far from the center of the spray field. On the other hand, the absolute velocities in the vertical direction (V_y) at the region closer to the center of spray are faster. The change of velocities in the vertical direction with the increase of injection pressure was much larger than that in the horizontal direction. The magnitude of velocities in the horizontal direction was much smaller than that in the vertical direction. Therefore, the trend in the speed of velocities (Fig. 12d) is the same as that of absolute velocities in the vertical direction.

The mean value of absolute velocities of total droplets over the six measuring points at different pressures is shown in Fig. 13. The tendency of velocities of total droplets showed almost the same behavior as that observed at each local region, as previously described.

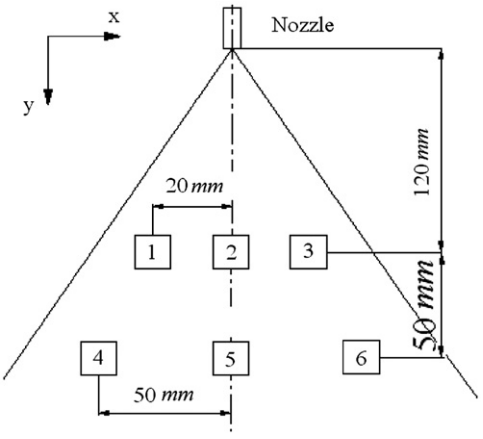

Fig. 9. Recording positions of spray field.

4.3. Sizing

Using the z coordinates of droplets, the holograms are reconstructed and the focused images of corresponding droplets are obtained. When the image is well-focused, the program automatically outlines the droplet and measures its information of size. The edge of droplet can be located and the number of pixels inside this edge is counted. Then, the properties of droplet size such as area and equivalent diameter are calculated. After reconstructing all particle images at different regions and distances, the sizing information of all droplets is easily obtained. Using the holograms in the previous section, the distribution of particle size is shown in Fig. 14. We can conclude that the droplet size is inversely proportional to the applied injection pressure, and the distribution of droplet sizes agrees well with Log-normal distribution.

The Sauter mean diameters, D_{32}, at different regions in the spray field at different pressures are shown in Fig. 15. From the figure, we can clearly see that the droplet size is inversely

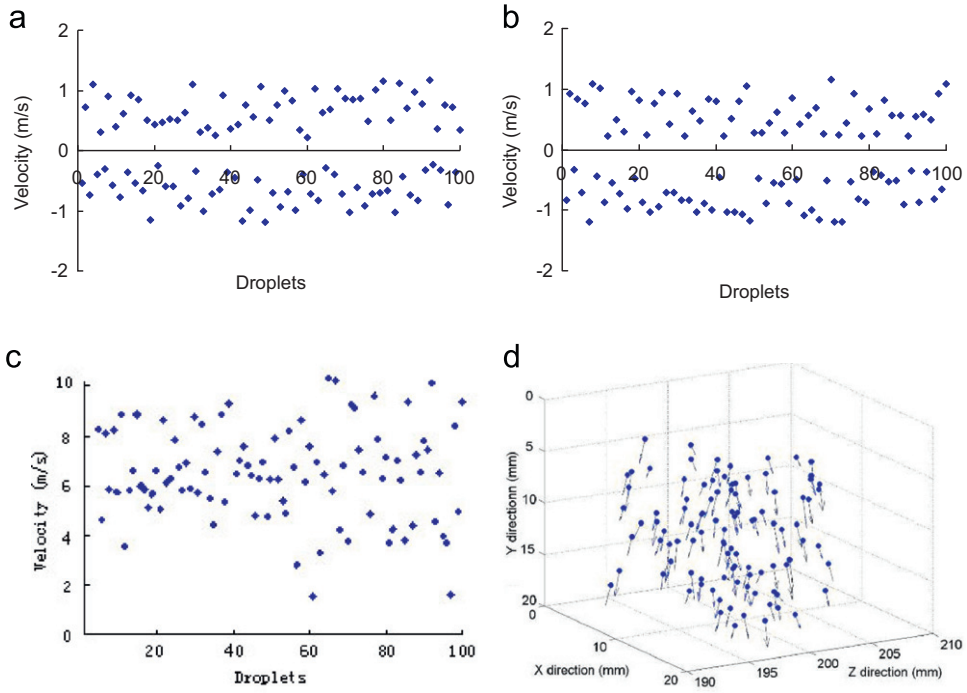

Fig. 11. Typical distribution of droplet velocities in the *x*, *y*, and *z* directions for Fig. 10; (a) *x* direction, (b) *y* direction, (c) *z* direction, and (d) velocity vectors in 3-D coordinate.

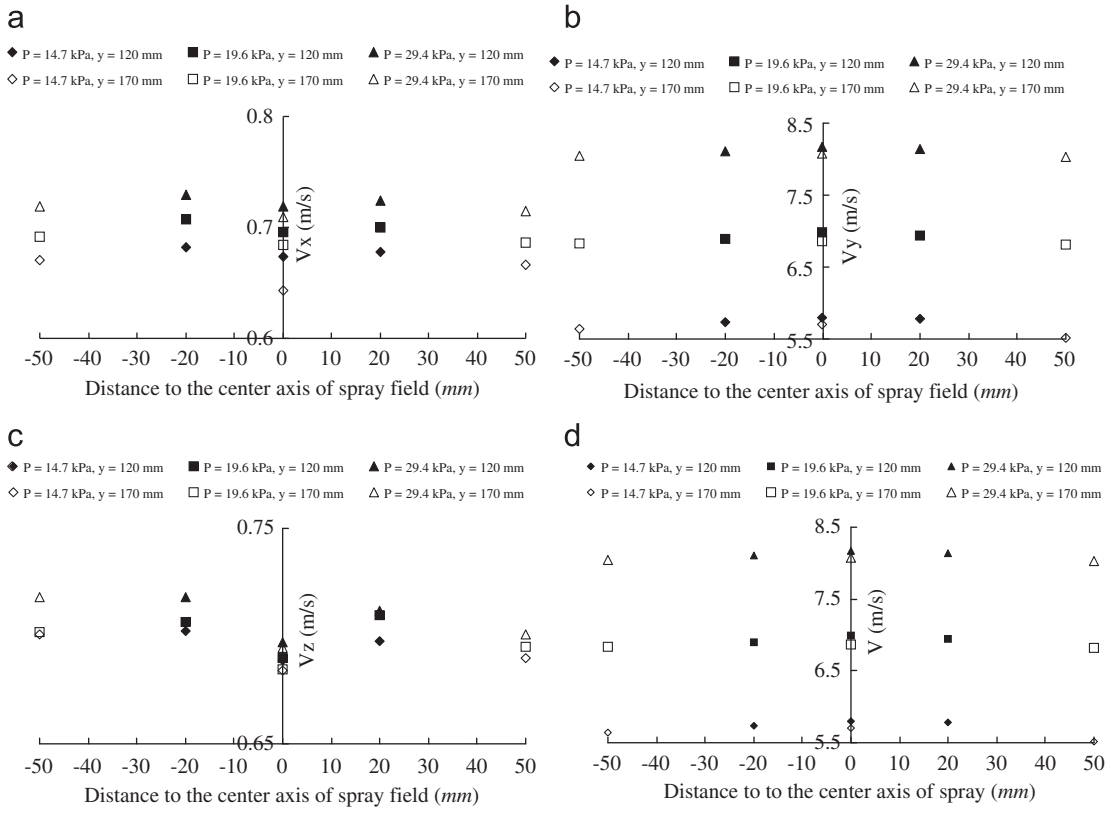

Fig. 12. Absolute velocities of droplets; (a) *x* coordinate, (b) *y* coordinate, (c) *z* coordinate, and (d) magnitude of velocities.

proportional to the applied injection pressure. Fig. 15 also shows that the size of droplets in the center axis of the spray is smaller than those in the sides of the spray. These results are consistent with the behavior expected in typical sprays.

4.4. Comparison

To verify the feasibility of a digital particle holographic system for measurement of a spray field, a particle dynamics analyzer

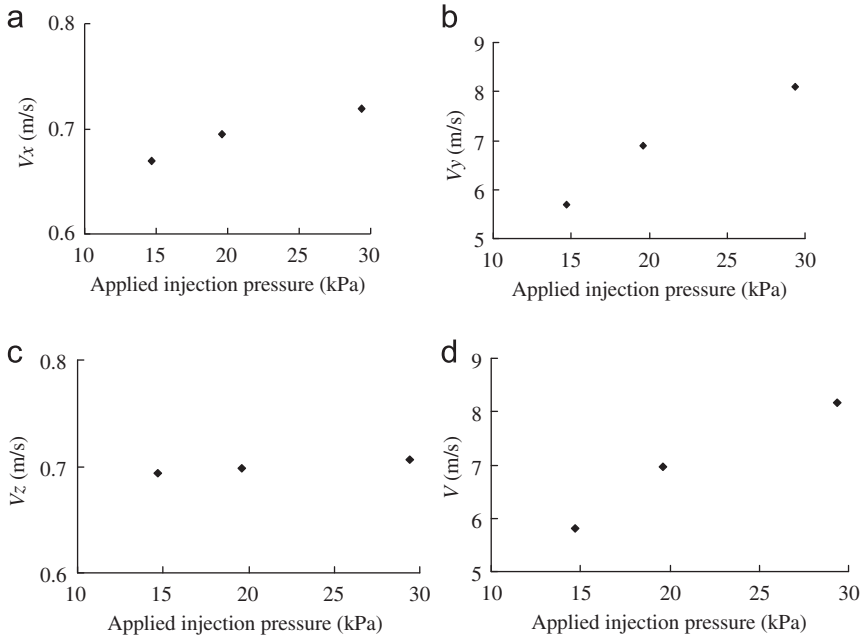

Fig. 13. Mean of absolute velocities of overall droplets; (a) *x* direction, (b) *y* direction, (c) *z* direction, and (d) magnitude of velocities.

(PDA, Dantec) was applied to a spray field under the same conditions as those used with the holographic method. In PDA measurements, only one point, which is rough at the center of the region, is measured. So, the velocities and the sizes of points, which were rough at the center of regions shown in Fig. 9 were compared.

A comparison of size and velocity measurements in the *y* direction between these two techniques is shown in Fig. 16. The difference in the velocity measurement results between the two methods is quite significant in all the regions at low injection pressures. As the pressure increased, the results are almost the same at regions close to the nozzle (1, 2, and 3 in Fig. 7), and there is a slight difference at regions far from the nozzle (4, 5, and 6 in Fig. 7). This tendency also appeared in the size measurement. The difference between the two methods is large at low pressures, but becomes smaller as the pressure increases. Fig. 17 compares the mean velocity of overall spray droplets in the *y* direction between DH and PDA.

Except some differences appearing at low pressure, the measurement results obtained by PDA and DH are almost similar based on the preceding observations. The digital holographic technique is superior to the PDA approach because it can capture information in a test volume with a simple setup, high efficiency, and the ability for real time analysis.

4.5. Uncertainty analysis

Firstly, the depth resolution and the lateral resolution of our system are discussed here. The depth resolution, δ_z, and the lateral resolution, δ_r, can be determined by [16]

$$\delta_z = 1.77\frac{\lambda}{NA^2}$$
$$\delta_r = \frac{\lambda}{2NA} \tag{7}$$

The numerical aperture (NA) is given by [12]

$$NA = \frac{W}{2\sqrt{(W/2)^2+d^2}} \tag{8}$$

where W is the CCD width and d is the object distance.

In our study, the CCD width, W, is 2048 (pixels) × 7.4 μm (pixel size). The object distance is roughly from 150 to 250 mm based on the region of spray filed. So, the NA value of our system is from 0.03 to 0.05 yielded by Eq. (8). Combining the NA value and Eq. (7), the depth resolution, δ_z, and the lateral resolution, δ_r, can be obtained as follows: the interval of the depth resolution, δ_z, is [376–1046 μm]; the interval of the lateral resolution, δ_r, is [5.32–8.86 μm].

As discussed before, the reconstruction interval, Δz, was chosen as 10 μm. This ensures oversampling by at least 37 in the z direction and it can improve the longitudinal particle resolution. The pixel size of CCD is 7.4 μm, which is also enough corresponding with the interval of the lateral resolution.

The particle velocity, V, are calculated by

$$V = \sqrt{V_x^2+V_y^2+V_z^2} \tag{9}$$

where V_x, V_y, and V_z are the particle velocities in each direction, respectively. The components of particle velocity in each direction are calculated by division of moved distances, D, by the time interval of double expose, Δt. For x and y directions, the distance moved by particle were obtained by multiplying the number of pixels between the center of particles at each exposure, ΔN, by the pixel size of CCD, Δ. They are expressed by

$$V_i = D_i/\Delta t = \Delta N_i \Delta i/\Delta t \quad i = x,y \tag{10}$$

For z directions, the distance moved by particle was the difference of the focal plane of the particles at each expose. The velocity can be described as

$$V_z = (d_2-d_1)/\Delta t \tag{11}$$

where d_1 and d_2 are the focal planes of the particle along z direction in each exposure.

The uncertainty of the particle velocity is expressed as the first one of Eq. (12).

$$u_V = \sqrt{\frac{V_x^2u_{V_x}^2+V_y^2u_{V_y}^2+V_z^2u_{V_z}^2}{V_x^2+V_y^2+V_z^2}}$$
$$u_{V_i} = \sqrt{\left(\frac{\Delta N_i}{\Delta t}u_{\Delta i}\right)^2+\left(\frac{\Delta N_i\Delta i}{\Delta t^2}u_{\Delta t}\right)^2+\left(\frac{\Delta i}{\Delta t}u_{\Delta N_i}\right)^2} \quad i = x,y$$

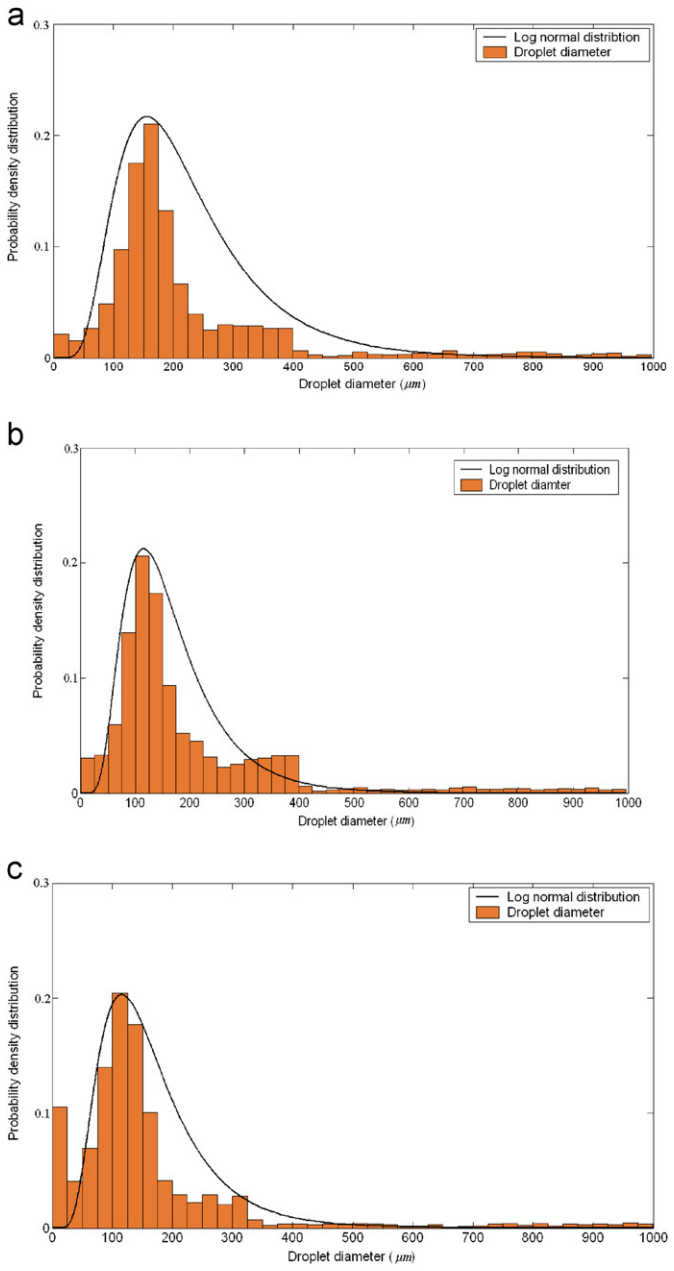

Fig. 14. Distribution of droplet sizes; (a) P=14.7 kPa, (b) P=19.6 kPa, and (c) P=29.4 kPa.

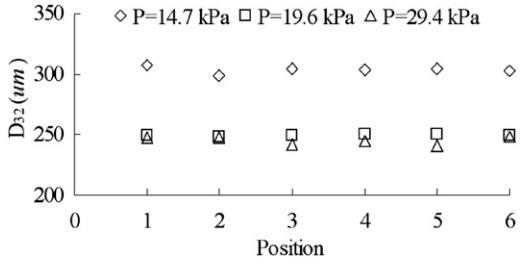

Fig. 15. Sauter mean diameters of spray droplets.

$$u_{V_z} = \sqrt{\frac{u_{d_2}^2 + u_{d_1}^2}{\Delta t^2} + \frac{(d_2 - d_1)^2}{\Delta t^4} u_{\Delta t}^2} \tag{12}$$

In Eq. (12), the uncertainty of time interval of double exposure, $u_{\Delta t}$, approximate to zero because of the precision of the pulse

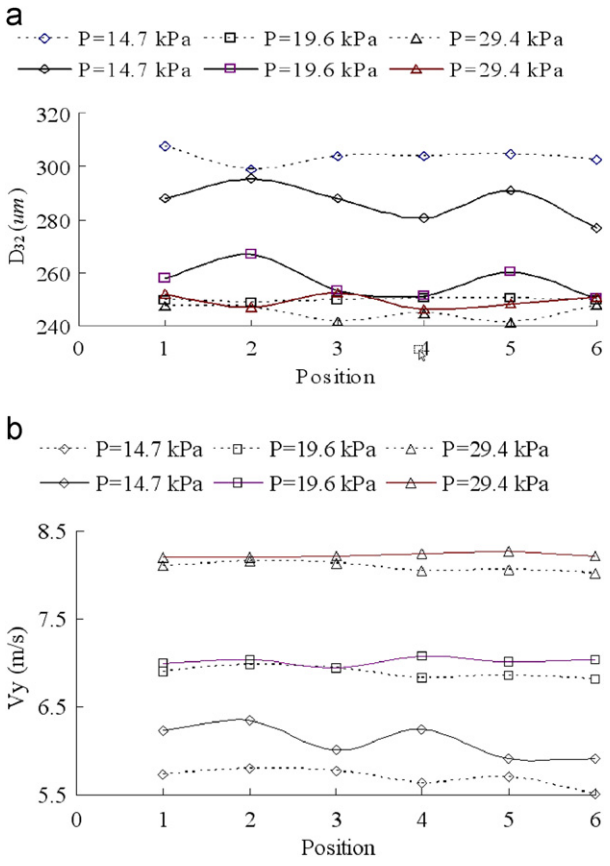

Fig. 16. Comparison of (a) size and (b) velocity in y direction measurement between DH and PDA (PDA: solid line, DH: dotted line).

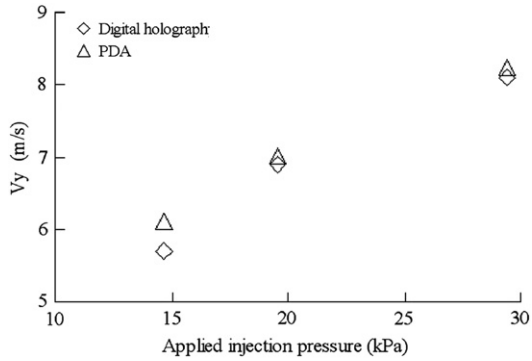

Fig. 17. Comparison of mean velocity of overall spray droplets in the y direction between DH and PDA.

generator and the laser machine; the uncertainty of number of pixels, $u_{\Delta N_i}$, was assumed to be ± 1 pixel; the uncertainty of pixel size, $u_{\Delta i}$, was assumed to be zero. The uncertainty of the focal plane position, u_{d1} and u_{d2}, can be obtained by the calibration target. After calculating the focal plane of particles in target 10 times, we obtained the uncertainty of the focal plane position, ± 9.9 μm by the method of type A evaluation of standard uncertainty.

Based on the above results, the uncertainties of the velocities of particles are calculated. The maximum is ± 0.296 m/s, which is $\pm 3.25\%$ of measured value. The mean of uncertainty is 0.293 m/s. The uncertainty of particle diameter was also obtained by the calibration target. We calculated the particle area by multiplying

Table 3
Comparison of actual diameters and measured values.

Actual diameter (μm)	300	230	160	100	70	31
Measured diameter (μm)	322.49 ± 1.55	233.52 ± 1.02	161.71 ± 0.59	101.67 ± 0.84	71.045 ± 0.50	31.229 ± 0.98
Error (μm)	22.49	3.52	1.71	1.67	1.05	1.23

the pixel number in image by the unit area of pixel, and then obtained the diameter of particle. After measurement of different particles 10 times, the calculated uncertainties of particle diameters are shown in Table 3. The maximum uncertainty is ± 1.55 μm, which is $\pm 0.4\%$ of the measured value. The maximum of errors is 22.49 μm, which is 7.49% of the actual diameter.

5. Conclusions

The potential of digital particle holography in spray field measurements was evaluated in this study. An experimental setup, which is based on the simplest in-line optical configurations to record spray field holograms at two different times was established with a synchronization system for time control. Using the system, many double pulse holograms in different regions of a spray field and at different pressures were captured. To process recorded holograms, the correlation coefficient method was used for focal plane determination of particles. For noise removal in digital particle holography, a Wiener filter was applied to the hologram and the reconstruction image, respectively. Experimental results proved that this filter can efficiently remove noise and increase the precision of focal plane location by the correlation coefficient method. For post-processing of reconstruction images, the two-threshold method and the image segmentation technique were presented and used effectively in binary image transformation. After binarization of each double exposure image, the spatial positions of the droplets were easily located. The match probability method was adopted for particle pairing and the droplet velocities were evaluated. Based on this simple system and these special methods, the 3-D velocity and the size features of spray droplets were measured successfully. The measurement results of the digital holographic system were compared to those made using common laser instruments. The comparison showed that the digital particle holographic system and these methods work well for various droplet concentrations, and that the measurement errors are acceptable.

Acknowledgement

This work was supported by the Korea Research Foundation Grant funded by the Korean Government (KRF-2008–313-D00137), by the Natural Science Foundation Project of CQ CSTS (2010BB2087), by the Natural Science Foundation Project of CQ EC(KJ110822), and by the Priming Scientific Research Foundation of CQUT(2009zd29).

References

[1] Durst F, Melling A, Whitelaw JH. Principles and Practices of Laser-Doppler Anemometry. London: Academic Press; 1981 Laser-Doppler Anemometry.
[2] Hinsch KD. Speckle Metrology. New York: Marcel Dekker; 1993. White Light Speckle Metrology.
[3] Jones AR, arjeant SM, Davis CR, Deham RO. Application of in-line holography to drop size measurement in dense fuel sprays. Appl Opt 1978;17:328–30.
[4] Shimizu I, Shimoda M, Suzuki T, Emori Y. A light scattering and holographic technique for determining droplet size and volume density distribution in diesel fuel sprays. SAE Paper 820355, 1982.
[5] Muller J, Kebbel V, Juptener W. Characterization of spatial particle distributions in a spray-forming process using digital holography. Meas Sci Technol 2004;15:706–10.
[6] Palero V, Arroyo MP, Soria J. Digital holography for micro-droplet diagnostics. Exp Fluids 2007;43:185–95.
[7] Lee J, Sallam KA, Lin KC, Carter CD. Spray structure in near-injector region of aerated jet in subsonic crossflow. J Propulsion Power 2009;25:258–66.
[8] Lee J, Miller B, Sallam KA. Demonstration of digital holographic diagnostics for the breakup of liquid jets using a commercial-grade CCD sensor. Atomization Sprays 2009;19:445–56.
[9] Miller B, Sallam KA, Bingabr M, Lin KC, Carter CD. Breakup of aerated-liquid jets in supersonic crossflows. J Propulsion Power 2008;24:253–8.
[10] Christoph TK, Axel L. Off-axis and in line electron holography: a quantitative comparison. Ultramicroscopy 2010;110:460–71.
[11] Schnars U, Jueptner W. Digital Holography. Berlin: Springer; 2005. Digital Holography.
[12] Garcia-Sucerquia J, Xu W, Jericho SK, Klages P, Jericho MH, Kreuzer HJ. Digital in-line holographic microscopy. Appl Opt 2006;45:836–50.
[13] Yang Y, Kang BS. Application of digital holography to sprays. In: Proceedings of Asia Display 2007, pp. 2050–4.
[14] Denis L, Fourner T, Ducottet C. Twin-image noise reduction by phase retrieval in in-line digital holography. Proc SPIE 2005;5914:148–61.
[15] Singh VR, Asundi AK. Amplitude contrast image enhancement in digital holography for particles analysis. Proc SPIE 2005;5878:17.1–8.
[16] Meinecke T, Sabitov N, Sinzinger S. Information extraction from digital holograms for particle flow analysis. Appl Opt 2010;49:2446–55.
[17] Kim S, Lee SJ. Effect of particle concentration on digital holographic PTV measurement. J Korea Soc Mech Eng B 2006;30:929–34.
[18] Francisco P, Edison G, Jorge R, Jose LV. Adaptive filter to improve the performance of phase-unwrapping in digital holography. Opt Commun 2004;238:245–51.
[19] Jain AK. Fundamentals of Digital Image Processing. Englewood Cliffs: Prentice-Hall; 1989.
[20] Lefebvre CB, Coëtmellec S, Lebrun D, Özkul C. Application of wavelet transform to hologram analysis: three-dimensional location of particles. Opt Lasers Eng 2000;33:409–21.
[21] Dubois F, Schockaert C, Callens N, Yourassowsky C. Focus plane detection criteria in digital holography microscopy by amplitude analysis. Opt Express 2006;14:5895–980.
[22] Yu L, Cai L. Iterative algorithm with a constraint condition for numerical reconstruction of three-dimensional object from its hologram. J Opt Soc Am A 2001;18:1033–45.
[23] Choo YJ, Kang BS. The characteristics of the particle position along an optical axis in particle holography. Meas Sci Technol 2006;17:761–70.
[24] Yang Y, Kang BS, Choo YJ. Application of the correlation coefficient method for determination of the focal plane to digital particle holography. Appl Opt 2008;47:817–24.
[25] Baek SJ, Lee SJ. A new two-frame particle tracking algorithm using match probability. Exp Fluids 1996;22:23–32.